Magnetic Properties of Bulk Nanocrystalline Cobalt Ferrite Obtained by High-Pressure Field Assisted Sintering

Angelica Baldini[1], Michele Petrecca[2,3], Claudio Sangregorio[3], Umberto Anselmi-Tamburini[1]

[1]Dipartimento di Chimica, Università di Pavia, V.le Taramelli 12, 27100 Pavia, Italy
[2]Dipartimento di Chimica, "Ugo Schiff", Università degli Studi di Firenze, via della Lastruccia 3-13, I-50019 Sesto Fiorentino, and Consorzio INSTM, via Giusti 9, I-50121 Firenze, Italy
[3]I.C.C.O.M. - CNR, via Madonna del Piano 10, I-50019 Sesto Fiorentino, and Consorzio INSTM, via Giusti 9, I-50121 Firenze, Italy

E-mail: angelica.baldini01@universitadipavia.it

Received xxxxxx
Accepted for publication xxxxxx
Published xxxxxx

Abstract

Nanometric cobalt ferrite has been investigated extensively due to its unique combination of magnetic properties. Most of these investigations are focused on the properties of nanopowders or individual nanoparticles. However, the possibility of obtaining bulk materials retaining the magnetic properties of the nanopowders is relevant for several technological applications. The production of nanostructured bulk magnetic materials received limited attention. In particular, the role of the microstructure in determining the magnetic properties of the final material is still poorly understood. In this work, we investigated the use of cobalt ferrite nanopowders produced using a simple, inexpensive, water-based method for the production of bulk nanostructured ferrites. The nanopowders, presenting a strong agglomeration, have been densified by high-pressure field-assisted sintering (HP-FAST). Different sintering conditions and powder treatments have been used to obtain materials with a spectrum of complex microstructures. We observed that the best magnetic properties are not necessarily associated with the more uniform microstructure. The magnetic properties of the obtained macroscopic objects, made of nanometric cobal ferrite grains, are really promising if compared with the literature.

Keywords: Nanopowders, sintering, bulk material, cobalt ferrite, microstructure

1. Introduction

Hard magnetic materials represent a crucial component in a large number of relevant technological applications. The best hard magnetic properties are presented by alloys, such as rare earth (RE) alloys containing neodymium or samarium [1-3] or, to a minor extent, ALNICO. However, the limited availability and the rising cost of RE metals [4], together with their chemical instability and low resistance to corrosion, have recently fuelled the interest towards alternative magnetic materials. Ceramic oxides represent an attractive alternative, as they do not suffer from oxidation or corrosion, are widely available, inexpensive, and environmentally friendly. However, the magnetic properties in magnetic oxides are still largely inferior to RE-based magnetic alloys. On the other hand, it has been shown that the nanostructure can significantly alter the magnetic properties of these oxides. [5-8] The nanostructure, in fact, can drastically modify the

 © xxxx IOP Publishing Ltd

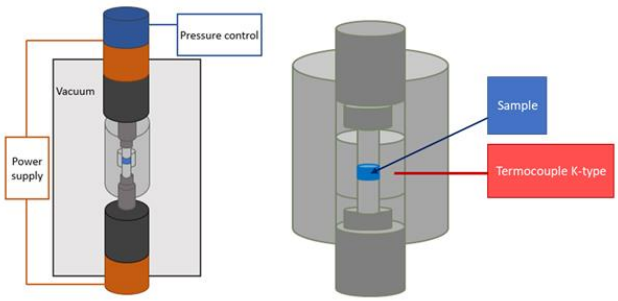

Figure 1. Schematic illustration of the HP-FAST apparatus.

magnetization, the magnetic anisotropy, and the ordering (Curie and Néel) temperature of the magnetic material. [9,10] In particular, it is well known that the highest coercivity is obtained at the single to multidomain threshold, which for the most common magnetic materials falls in the 10-150 nm range. Such property is appealing for designing a permanent magnet, since a large coercivity is required to sustain the residual magnetization. The unusual magnetic properties exhibited by cubic ferrites nanoparticles (NP) have spurred a broad scientific interest over the last decades. [11,12] Cubic ferrites are compounds with a spinel crystal structure and general formula AB_2O_4, with A being a divalent cation and B Fe^{III}. [13,14] If compared to their micrometric counterpart, nanometric ferrites possess unusual saturation magnetization and higher coercive field. [15-17] One of the most promising spinel ferrite is cobalt-doped magnetite. Recently, 40 nm $Co_{0.6}Fe_{2.4}O_4$ nanoparticles have been proposed as a building block for the realization of permanent magnets (PM). [15] The substitution of Fe^{II} with the higher anisotropic ion Co^{II}, leads in fact to the increase of the coercivity, with respect to magnetite, without significantly affecting the saturation magnetization.

The magnetic properties of monodispersed nanopowders or nanocrystals have been extensively investigated, [18-25] but most technological applications require materials to be in bulk form. For this reason, the production of macroscopic bulk objects retaining the magnetic properties of the nanopowders is highly desirable. Despite that, the number of reports on cobalt ferrite bulk nanostructured materials is still quite limited. [26-30] The main challenges are represented by the control of grain growth during the sintering process and the preservation of the crystal structure. However, it has been recently shown that innovative fast sintering methods, such as Field Assisted Sintering (FAST) or Spark Plasma Sintering (SPS), offer the possibility to obtain the full densification of nanopowders while maintaining a very limited grain growth. [31-33] The use of high pressures (up to 1 GPa) coupled with fast sintering cycles has demonstrated to be particularly effective, even when low-quality nanopowders, presenting a high level of agglomeration, are used as starting materials. [34] Most studies on the magnetic properties of ferrite nanomaterials rely on synthesis methods that are designed to produce high-quality, monodisperse nanopowders. [18,35,36] These methods, however, are generally expensive, time-consuming, and present very low yields. As such, they do not represent an ideal source of nanopowders for the realization of materials in bulk form. On the other hand, simpler and high-yield methods, such as the Pechini method, [37] generally produce badly agglomerated nanopowders that are considered not ideal for sintering.

This work aimed to fill the gap by exploring the possibility to prepare bulk nanostructured $CoFe_2O_4$ samples by high-pressure field-assisted sintering (HP-FAST) starting from nanopowders produced using a simple, low-cost approach based on a modified Pechini synthesis and to characterize their magnetic properties.

2. Methods

2.1 Synthesis of ferrite NP

Cobalt ferrite nanopowder has been synthesized using a modified Pechini method. $Fe(NO_3)_3 \cdot 9H_2O$, $Co(NO_3) \cdot 6H_2O$ with cationic stoichiometry 2:1 and citric acid, with a molar ratio equal to 1.1 with respect to the sum of the cations, were dissolved in 60 mL of distilled water. The solution was kept under stirring at 80 °C for 16 h until a brown gel was formed. This gel was dried in a furnace at 120 °C for 2 h, then transferred into an alumina crucible and calcined at 600 °C for 1 h. The product is represented by a strongly agglomerated black powder. In some cases, a mild milling treatment was performed using a FRITSCH Premium line P7 ball-miller with WC jars and balls. The jars were previously cleaned by milling 7 mL of SiO_2 powder at 400 rpm for 30 min.

2.2 Sintering process

Bulk nanostructured samples have been prepared using the home-made high-pressure field-assisted sintering (HP-FAST) apparatus, described in Figure 1. To achieve uniaxial pressures up to 1 GPa two-stage dies have been used. These composite dies include an external element, where most of the current flows and the heat is generated, made of high-density graphite and a second internal die, made of SiC or WC, allowing to obtain the high pressure. The combination of high pressures and high heating rates (200 °C/min) allows us to achieve a high level of densification with a minimum of grain growth. In a typical experiment, 0.150 g of nanopowders were placed in the double stage die with an internal diameter of 5 mm. The die was inserted in the HP-FAST apparatus and connected to a K-type thermocouple placed in its lateral wall. The HP-FAST chamber was evacuated to a pressure of 10 Pa. Two different experimental procedures have been followed. In one case a moderate uniaxial pressure (200 MPa) was initially applied to the sample, the temperature was increased linearly with a heating rate of 200 °C/min until the sample reached the

designated sintering temperature (T_{sint}, investigated range: 500 – 800 °C), and the pressure was then rapidly increased to the final value (P_{sint}, investigated range: 400 - 600 MPa). The sample was kept under these conditions for 5 min.

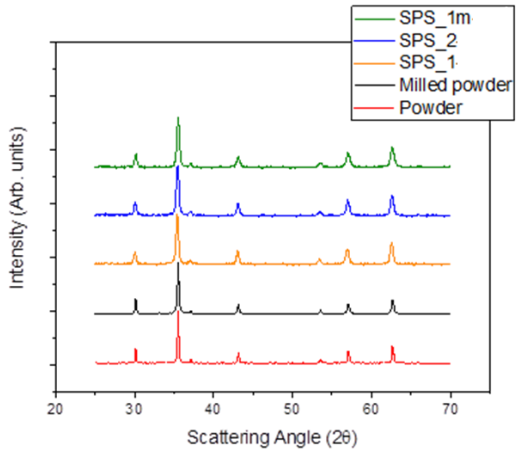

Figure 2 XRD patterns of the cobalt ferrite nanopowders and sintered samples.

At the end of the sintering cycle the pressure was quickly released, and the power supply turned off. In the following, the samples obtained using this procedure are labeled SPS_1. In the second procedure, the pressure was applied at the beginning of the process and maintained constant throughout the sintering cycle. The same range of pressure and sintering temperature as in the SPS_1 series were investigated. These samples are indicated by the label SPS_2. Samples obtained through the procedure SPS_1 starting from milled powders are indicated by the label SPS_1-m. In all cases, the sintered samples were discs of 5 mm in diameter and 1 mm thick.

2.3 Samples characterization

The densities of the sintered samples were determined at room temperature by immersion in EtOH using the Archimedes method. The density of cobalt ferrite grains was evaluated from crystallographic data. [38] The structural characterization was made by X-ray diffraction. XRD data were acquired on a Bruker D8 Advance diffractometer with Bragg-Brentano geometry, using a step size of *0.03°* (*2θ*) and an acquisition time of *5 s* per step. The microstructural characterization of the samples was performed using a high-resolution scanning electron microscope (SEM, TESCAN Mira 3) operated at 15-25 kV. The content of Fe and Co was determined by energy dispersive spectrometry (EDS, EDAX). Microstructural characterizations of the sintered materials have been performed on ceramographic sections. In this case, the sample was embedded in epoxy resin (Buehler EpoThin 2 Resin), sectioned, and polished. Before SEM analysis, all samples were coated with a carbon film using a Cressington carbon coater HR 208. The grain size of the nanopowder and of the sintered samples were calculated from the XRD pattern using the Scherrer equation and measured from SEM images using the software ImageJ. In this case, the reported values

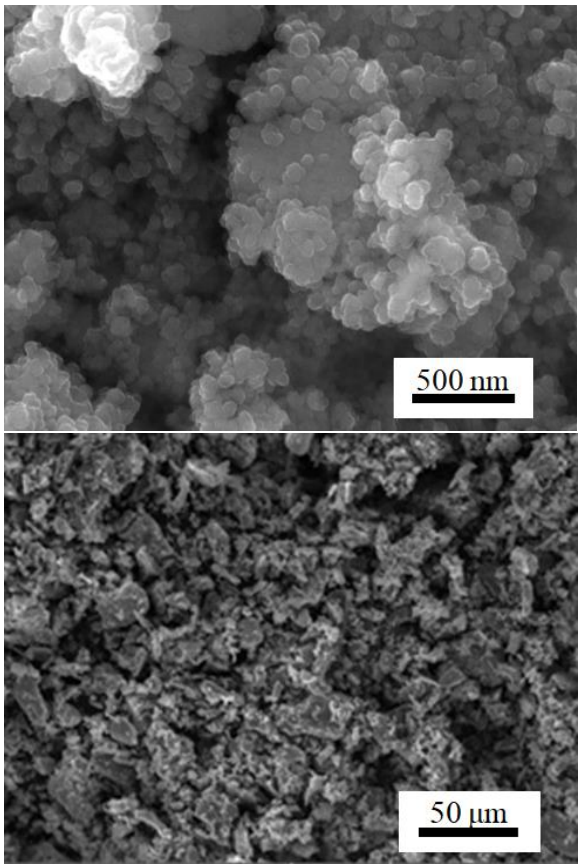

Figure 3: (a, top) SEM high-magnification and (b, bottom) SEM low-magnification images of the cobalt ferrite nanopowder.

represent the average of at least 100 grains for each sample. The magnetic measurements were carried out at room temperature on sintered discs, inserted with the axial direction (i.e., the normal to the plane of the discs) perpendicular to the applied DC field. The magnetic response was recorded as a function of the applied field using a Physical Property Measurement System (PPMS) with a Vibrating Sample Magnetometer (VSM) by Quantum Design Inc. The energy product (BH_{max}) value was estimated from the BH curve, using the disc measured density and a demagnetizing factor of 0.1, according to the value reported in the literature for the same geometry and orientation. [39]

3. Results and Discussion

3.1 $CoFe_2O_4$ nanopowders

The nanopowder synthesized using the modified Pechini method were single-phase $CoFe_2O_4$, as evidenced by the XRD

pattern reported in Figure 2. The lattice parameter *a*, calculated using the Pawley method, [40] was 0.8382(2) nm,

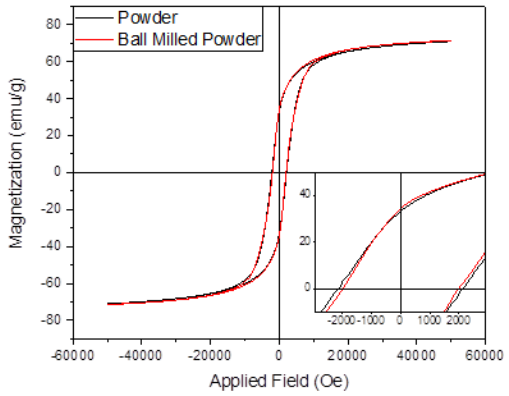

Figure 4 Hysteresis loops of the as-synthesized (black curve) and the ball-milled nanopowders (red curve).

a value comparable with that reported in the literature for stoichiometric cobalt ferrite, [38] while the crystallite size, as calculated from the XRD pattern, was ca. 45 nm. The average particle size was confirmed by HR-SEM analysis (Figure 3a). Low-magnification images (Figure 3b) evidenced the presence of an extensive agglomeration. It is worth to stress that the obtained average grain size is very close to the value for which the energy product of cobalt ferrite has been reported to be maximum. [15] The magnetic hysteresis loop recorded at room temperature on this nanopowder is reported in Figure 4, while a summary of the magnetic properties is reported in Table 1. The values for saturation magnetization (M_S, 71 emu/g), remnant magnetization (M_R, 33 emu/g) and coercive field (H_C, 2150 Oe) are comparable with the one reported in the literature for cobalt ferrite nanopowders obtained by various synthetic methods. [41-43] The BH_{max}, calculated considering the density of the stoichiometric cobalt ferrite (5.22 g cm^{-3}), and the sample shape (hand pressed pellet in Teflon tape with oriented with the normal perpendicular to the applied field, demagnetizing factor=0.05), was 6.0 kJ/m^3. The level of agglomeration decreased considerably after ball milling (see SI for SEM images), while the phase composition remained unchanged. The lattice parameter remained also constant (0.8384(2) nm), while a small decrease of the crystallite size, down to 35(5) nm, was observed. The hysteresis loop recorded at room temperature is shown in Figure 4, while the magnetic properties are summarized in Table 1. The saturation magnetization and the remanence remained almost unchanged (72 emu/g and 34 emu/g, respectively), while it was observed a slight decrease of the coercivity, from 2150 to 2000 Oe. The BH_{max} value was 6.2 kJ/m^3. These little differences are in the error range of the measurement technique (± 3 % on the magnetic moment value) and confirm that the milling process did not affect the crystallinity of the nanomaterial but decreased its agglomeration level.

3.2 $CoFe_2O_4$ sintered samples

Sintered samples were prepared using different combinations of temperature and pressure, using both as prepared and milled nanopowders. The sintering process did not produce modifications in the phase composition of the material that remained in all cases single-phase cobalt ferrites, as shown in Figure 2. The lattice parameters remained also unchanged (ca. 0.8385(2) nm), while the crystallite size could not be determined due to X-ray focalization errors, commonly observed when the sintered samples are analyzed, because they are too small considering the width of the x-rays beam and so it hits also the lateral surface. The dependence of the relative density of the samples (i.e. measured to bulk cobalt ferrite density ratio) on the sintering temperature is reported in Figure 5 for an applied pressure of 500 MPa, as a representative case. All samples obtained from the as prepared nanopowder densified at T ≥ 600 °C and presented a relative density above 95 %, reaching a maximum of 98 % at 700 °C.

Table 1 Structural and magnetic properties of the selected samples: coercive field (H_C), saturation magnetization (M_S) and remanent magnetization (M_r) recorded at room temperature and the calculated maximum energy product (BH_{max}); grain size evaluated by SEM images; relative density calculated as the ratio between the measured density and that of bulk cobalt ferrite.

	H_c (Oe) 300K	M_s (emu/g) 300K	M_r (emu/g) 300K	BH_{max} (kJ/m^3) 300K	Grain size SEM (nm)	Relative density (%)
Powder	2150	71	33	6,0	35(5)	-
Milled Powder	2000	72	34	6,2	35(5)	-
SPS_1-opt	1040	77	37	5,5	65(10)	90
SPS_2-opt	1000	73	30	3,8	55(10)	96
SPS_1-m-opt	2150	77	41	8,2	60(20)	96

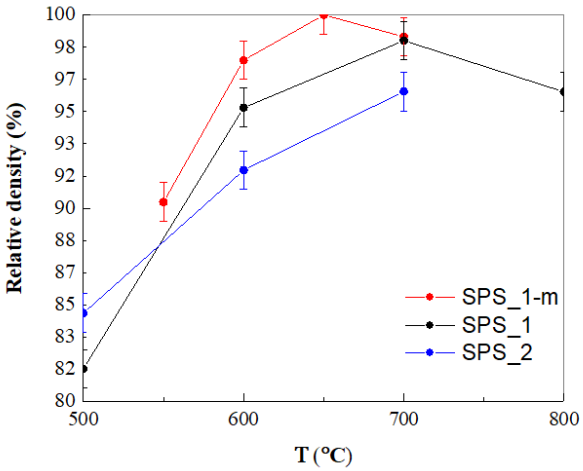

Figure 5 Relative density of the sintered samples for the series SPS_1, SPS_2, and SPS_1-m as a function of the sintering temperature. Uniaxial pressure: 500 MPa.

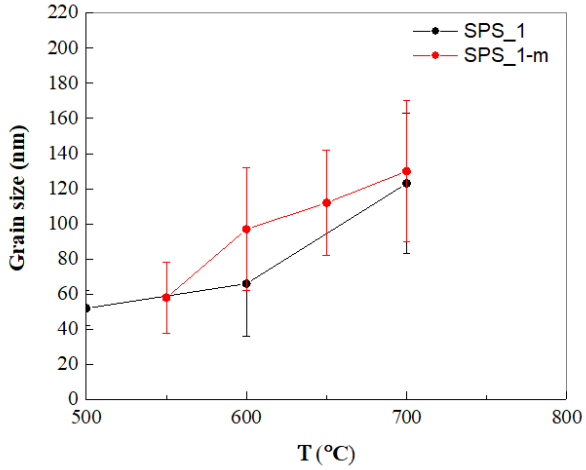

Figure 6 Grain size evaluated by SEM analysis of the sintered samples for the series SPS_1 and SPS_1-m as a function of the sintering temperature. Uniaxial pressure: 500 MPa.

Milled nanopowders, presenting a reduced agglomeration, were densified more efficiently (Figure 5). In this case full density was achieved at temperatures just above 600 °C using a pressure of 500 MPa.

It must be noted that pressure values of 400 MPa or higher are well above the typical values used in SPS or FAST processes, that are tens of MPa. However, such high pressure is essential to obtain high relative density values while keeping the sintering temperature and the sintering time low enough to avoid significant grain growth. Sintering times of only 5 minutes have been indeed used in this work. However, the data in Figure 6 show that even using such short times the grain size increases rapidly with the sintering temperature. In fact, the grain size increased from 50(10) nm to 120(40) nm when temperature is varied between 500 °C and 700 °C, for the SPS_1 series and from 60(20) to 130(40) for temperature increase from 550°C to 700 °C, for the SPS_1-m series.

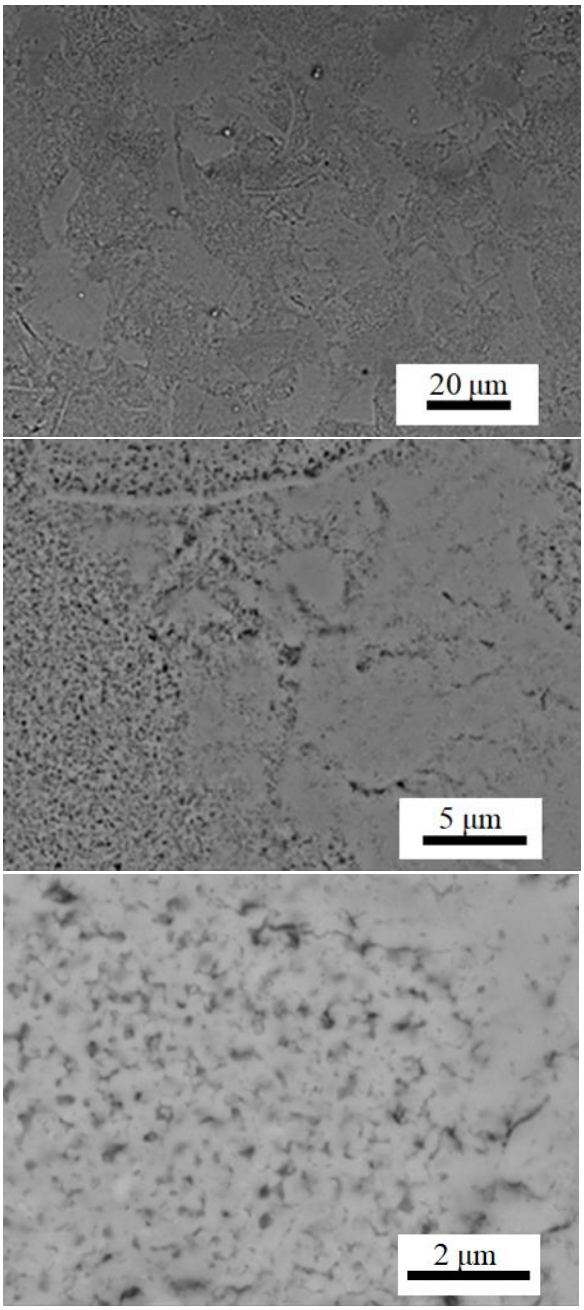

Figure 7 SEM images of a polished cross-section of SPS_1-opt. The detector used is a backscattered detector.

The optimal sintering conditions for the process carried out on the milled nanopowders were identified to be at T = 575 °C and P = 650 MPa. Using these conditions, indeed, it was possible to reach high relative density (97 %), while the grain size was still below 60 nm. The samples obtained using the SPS_2 procedure showed a maximum density at 700 °C (96 %). At higher temperature the material became too brittle. The microstructure of the sintered materials was strongly dependent on the type of starting nanopowders and on the sintering conditions.

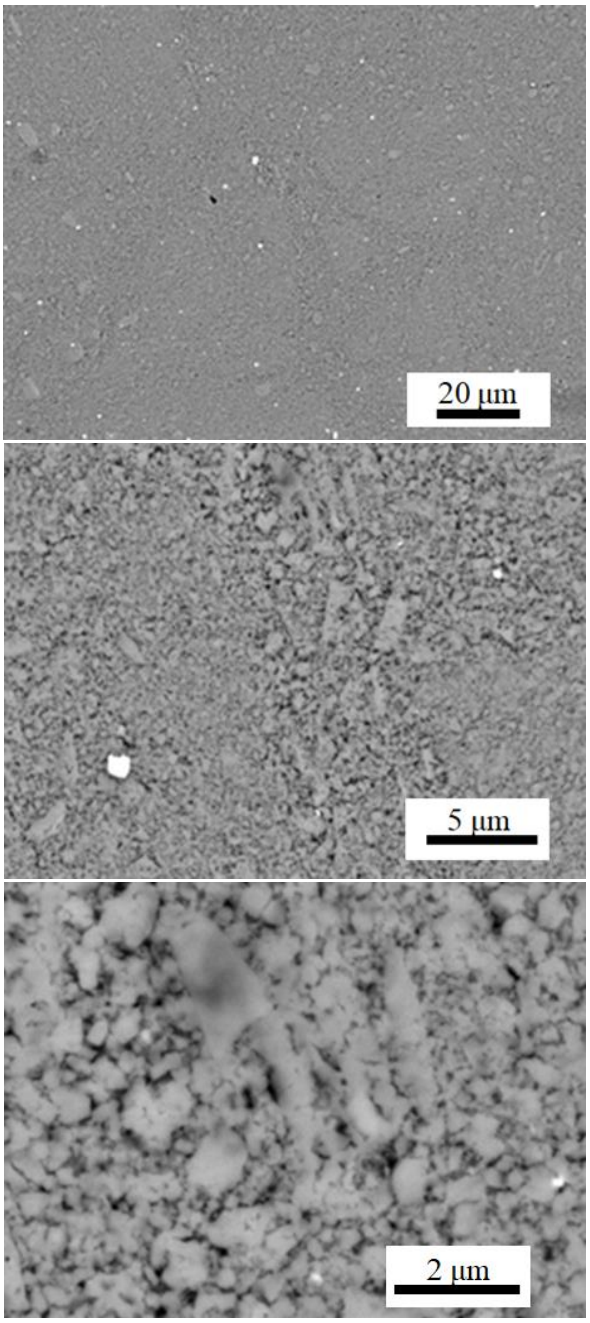

Figure 8 SEM images of a polished cross-section of SPS_1-m-opt. The bright spots correspond to amorphous WC deriving from the milling medium. The detector used is a backscattered detector.

Bulk samples obtained from unmilled nanopowder, using the procedure SPS_1 presented a quite inhomogeneous microstructure. SEM-BS images of polished cross-sections of a sample sintered at 575 °C and 650 MPa and show how the agglomeration present in the starting nanopowder was retained in the sintered material (Figure 7). The images show the presence of some fully dense areas, micrometric in size, surrounded by regions presenting residual nanoporosity. No macro or mesoporosity was observed. The use of a mild milling treatment considerably improved the homogeneity (Figure 8). The large agglomerates were not observed anymore, although higher magnifications images showed the evidence of a residual agglomeration, sub-micrometric in size, together with some nanoporosity. Notably, the samples that underwent milling treatment always showed the presence of contamination from amorphous WC, deriving from the milling medium. The presence of this impurity was confirmed by the SEM analysis using EDS.

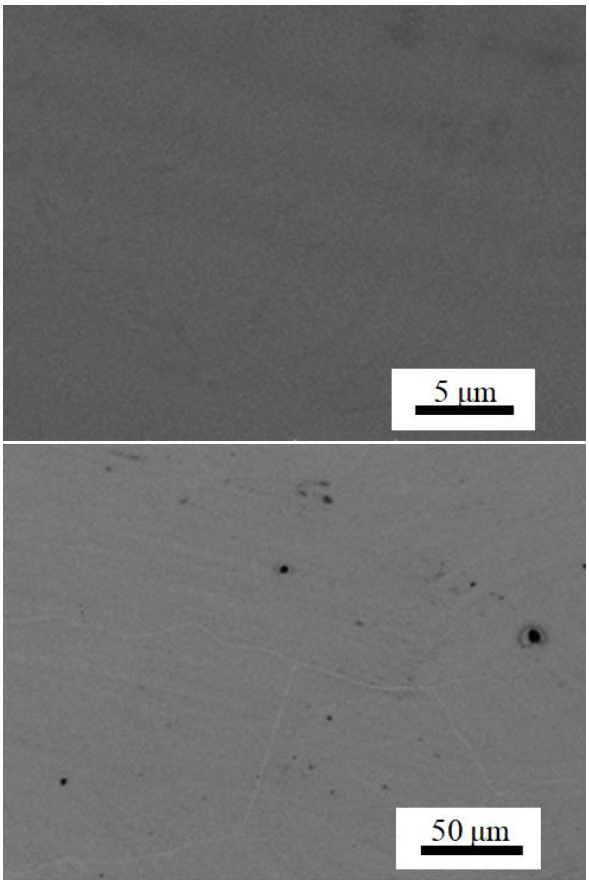

Figure 9 SEM images of a polished cross-section of SPS_2-opt. The detector used is a backscattered detector

A much more uniform microstructure was obtained using the densification strategy SPS_2. In this case, the maximum uniaxial pressure was applied at the beginning, and it was maintained throughout the entire sintering cycle. In this way, the agglomerates were drastically reduced, as they were probably effectively crushed in the early stages of the process, where plastic deformation was still not possible (Figure 9).

In order to determine which procedure provide the samples with the best magnetic properties, we investigated in detail three samples belonging to the different series prepared by keeping constant the sintering parameters (T_{sint} = 575 °C and

P_{sint} = 650 MPa). These samples are called SPS_1-opt, SPS_2-opt and SPS_1-m-opt.

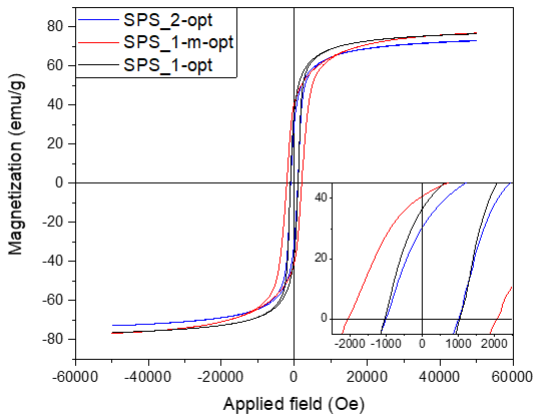

Figure 10 Hysteresis loop for the sintered samples SPS_1-opt, SPS_2-opt, and SPS_1-m-opt.

The magnetic properties of the optimized samples produced during this investigation are summarized in Table 1, while Figure 10 shows the hysteresis loops measured at room temperature. First of all, it is instructive to compare the properties of the sintered samples with the nanopowders: for samples SPS_1-m-opt and SPS_1-opt both M_S and M_R at 300 K increased after sintering up to 77 emu/g and 48 emu/g, respectively. Conversely, no increase is observed for SPS_2-opt. The coercive field instead decreased in the sintered samples SPS_1-opt and SPS_2-opt to ca. 1000 Oe but not in SPS_1-m-opt, where it remained comparable to the starting nanopowder (2150 Oe). Consequently, the maximum energy product, evaluated using the density of the sintered pellet, is lowest for SPS_2-opt (3.8 kJ/m^3), slightly increases for SPS_1-opt (5.5 kJ/m^3) and reach the highest value of 8.2 kJ/m^3 for SPS_1m-opt, with an increase respect to the starting nanopowder of ca 30 % (6.2 kJ/m^3). However, it deserves to be noted that a comparison with BH_{max} obtained on powder sample is hampered by the fact that the latter was estimated using the particle density and not the actual density of the pellet (unknown), and thus is overestimated. Finally, it is worth to mention that the values of the magnetic parameters we observed in our sintered samples were, in most cases, superior to those reported in the literature for densified cobalt ferrite materials [26-30,42,43] as described in Table 2. Particularly relevant is the considerable higher values of H_C observed in the case of deagglomerated powder (SPS_1-m-opt).

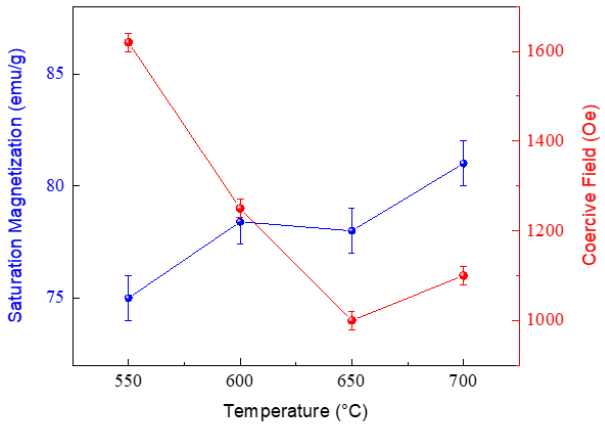

Figure 11 Coercive field and saturation magnetization for the sintered samples of the series SPS_1-m as a function of the sintering temperature.

Table 2 Comparison of the magnetic properties with the literature.

	H_c (Oe) 300K	M_s (emu/g) 300K	Grain size (nm)	Relative density (%)
This study	750-2150	70-86	45-150	88-100
[28]	239	78.9	120	97
[28]	666	70.0	100	97
[29]	640	79.3	28	91
[26]	222	83	71	97
[27]	580	51	10	92
[27]	525	69	12-15	93
[27]	660	70	40-50	93
[30]	826.1	82.1	<200	/

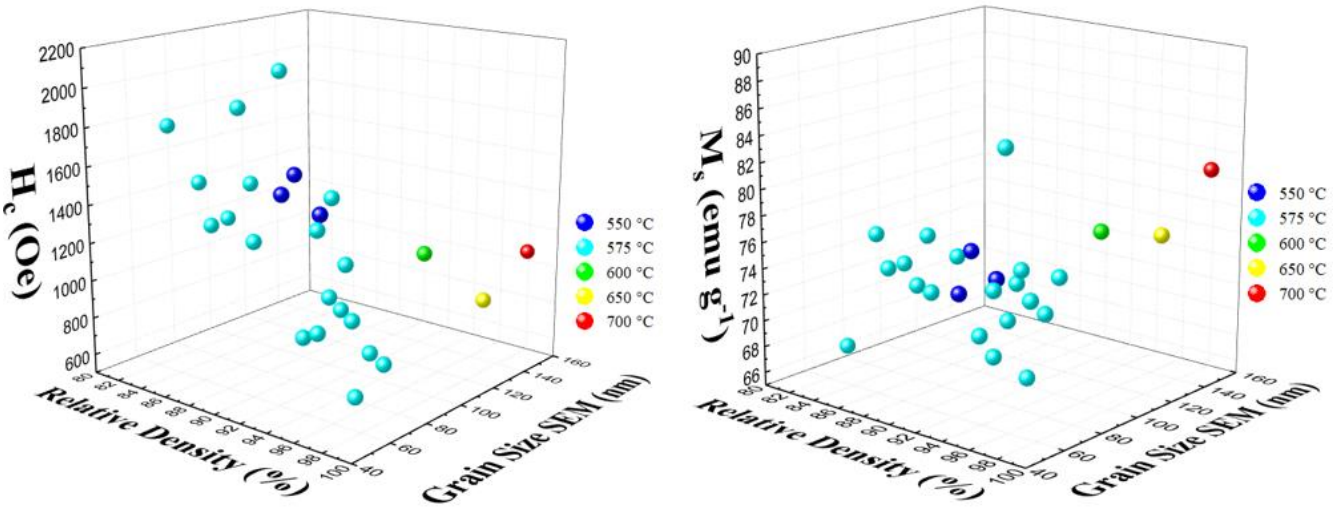

Figure 12 Coercive field and saturation magnetization as a function of the relative density and grain size for all the sintered samples produced in this work.

This result suggests that the microstructure plays an important role in determining the magnetic properties of the final sintered product. Surprisingly, a very uniform microstructure does not seem to be particularly advantageous to this goal. In fact, samples SPS_2-opt, which is characterized by a very homogeneous microstructure, presents a lower BH_{max} than SPS_1-opt, which has comparable relative density and grain size, but a very inhomogeneous microstructure, characterized by the presence of large agglomerates. On the other hand, SPS_1-m-opt shows the best magnetic properties, particularly regarding the coercive field, although the material presents an intermediate agglomeration and contains some contamination from the milling medium. Apparently, the material obtained using this procedure presents the best microstructure, in terms of grain size, relative density, and separation between the grains, to maximize loop area.

Some further insight on the role played by the microstructure in defining the magnetic properties can be obtained from the data in Figure 11. In these figures, the coercive field and saturation magnetizations for the material presenting the best combination of magnetic properties (SPS_1-m) are reported as a function of the sintering temperature in the range 550-700 °C. The coercive field and the magnetization presented an opposite trend: on increasing the sintering temperature the coercive field reduced to almost half the value of the starting powder, while M_S slightly increased.

To better identify the influence of structural parameters on the magnetic properties, H_C and M_S were plotted in 3D graphs as a function of the relative density and grains size (Figure 12) for all the sintered samples produced in this investigation. Despite some spreading in the data, the plot shows that, at least in the investigated range, the coercive field depends mainly on the relative density, being higher when the relative density is lower (the largest H_C values were obtained for density in the range 80-90 %). However, a small influence of the grain size is also observed. The behavior of the magnetization is more complex: fully dense materials present the highest M_S, while no clear trend with the grain size emerged.

4. Conclusions

We demonstrated that high-pressure field-assisted sintering (HP-FAST) allows obtaining almost fully dense cobalt ferrite macroscopic objects maintaining a nanometric grain size, even when the starting nanopowders present a significant level of agglomeration. The use of very high uniaxial pressures, up to 600 MPa, allows obtaining a significant plastic deformation of the agglomerates, removing all macro- and mesoporosity even using relatively low sintering temperatures and times, reduced to few minutes. The magnetic properties of the starting nanopowders are almost entirely retained in the bulk samples when a mild milling treatment is used before compaction. On one hand we found that the presence of large agglomerates affects the magnetic properties of the sintered material, on the other some level of heterogeneity in the microstructure helps preserving to a certain extent, the appealing properties of the nanopowders As a matter of fact the material sintered following the SPS_1-m procedure exhibits a much larger energy product of the compacted powder.

The densification process introduces stronger interactions between the nanograins. Our results confirm that the role of these interactions in defining the magnetic characteristics of the sintered material is quite complex particularly in the case of materials presenting complex microstructures deriving from agglomerated nanopowders.

Acknowledgments

We acknowledge the CISRiC at the University of Pavia for the use of the HR-SEM facility and the European Commission for funds through project H2020 No. 720853 (Amphibian).

References

1. Elliott, R. Magnetic Properties of Rare Earth Metals. *Springer Science & Business Media*, (2013).
2. Koehler, W. C. Magnetic Properties of Rare-Earth Metals and Alloys. *J. Appl. Phys.* **36**, 1078–1087 (1965).
3. Sagawa, M., Fujimura, S., Yamamoto, H. & Hiraga, K. Permanent magnet materials based on the rare earth-iron-boron tetragonal compounds. *IEEE Trans. Magn.* **20,** 1584-1589 (1984)
4. Massari, S. & Ruberti, M. Rare earth elements as critical raw materials: Focus on international markets and future strategies. Resour. Policy 38, 36–43 (2013).
5. Gleiter, H. Nanostructured materials: basic concepts and microstructure. Acta Mater. 48, 1–29 (2000).
6. Moriarty, P. Nanostructured materials. Rep. Prog. Phys. 64, 297 (2001).
7. Cain, M. & Morrell, R. Nanostructured ceramics: a review of their potential. *Appl. Organomet. Chem.* **15**, 321–330 (2001)
8. Fernández-García, M., Martínez-Arias, A., Hanson, J. C. & Rodriguez, J. A. Nanostructured Oxides in Chemistry: Characterization and Properties. *Chem. Rev.* **104**, 4063–4104 (2004).
9. Trohidou, K. N. *Magnetic Nanoparticle Assemblies*. (CRC Press, 2014)
10. Issa, B., Obaidat, I., Albiss, B. & Haik, Y. Magnetic Nanoparticles: Surface Effects and Properties Related to Biomedicine Applications. *Int. J. Mol. Sci.* **14**, 21266–21305 (2013)
11. Mathew, D. S. & Juang, R.-S. An overview of the structure and magnetism of spinel ferrite nanoparticles and their synthesis in microemulsions. *Chem. Eng. J.* **129**, 51–65 (2007).
12. Pacakova, B., Kubickova, S., Reznickova, A., Niznansky, D. & Vejpravova, J. Spinel Ferrite Nanoparticles: Correlation of Structure and Magnetism. *Magn. Spinels - Synth. Prop. Appl.* (2017) doi:10.5772/66074.
13. Carta, D. Casula, M. F., Falqui, A., Loche, D., Mountjoy, G., Sangregorio, C. & Corrias, A. A Structural and Magnetic Investigation of the Inversion Degree in Ferrite Nanocrystals MFe_2O_4 (M = Mn, Co, Ni). *J. Phys. Chem. C* **113**, 8606–8615 (2009).
14. Verwey, E. J. W. & Heilmann, E. L. Physical Properties and Cation Arrangement of Oxides with Spinel Structures I. Cation Arrangement in Spinels. *J. Chem. Phys.* **15**, 174–180 (1947).
15. López-Ortega, A., Lottini, E., Fernández, C. de J. & Sangregorio, C. Exploring the Magnetic Properties of Cobalt-Ferrite Nanoparticles for the Development of a Rare-Earth-Free Permanent Magnet. *Chem Mater.* **27**, 4048–4056 (2015).
16. Vasilakaki, M., Ntallis, N., Yaacoub, N., Muscas, G., Peddis, D. & Trohidou, K.N. Optimising the magnetic performance of Co ferrite nanoparticles *via* organic ligand capping. *Nanoscale* **10**, 21244–21253 (2018).
17. Rondinone, A. J., Samia, A. C. S. & Zhang, Z. J. Superparamagnetic Relaxation and Magnetic Anisotropy Energy Distribution in $CoFe_2O_4$ Spinel Ferrite Nanocrystallites. *J. Phys. Chem. B* **103**, 6876–6880 (1999).
18. Baldi, G., Bonacchi, D., Innocenti, C., Lorenzi, G. & Sangregorio, C. Cobalt ferrite nanoparticles: The control of the particle size and surface state and their effects on magnetic properties. *J. Magn. Magn. Mater.* **311**, 10–16 (2007).
19. Joshi, H. M., Lin, Y. P., Aslam, M., Prasad, P. V., Schultz-Sikma, E. A., Edelman, R., Meade, T. & Dravid, V. P. Effects of Shape and Size of Cobalt Ferrite Nanostructures on Their MRI Contrast and Thermal Activation. *J. Phys. Chem. C* **113**, 17761–17767 (2009).
20. Li, S., John, V. T., O'Connor, C., Harris, V. & Carpenter, E. Cobalt-ferrite nanoparticles: Structure, cation distributions, and magnetic properties. *J. Appl. Phys.* **87**, 6223–6225 (2000).
21. Ayyappan, S., Panneerselvam, G., Antony, M. P. & Philip, J. High temperature stability of surfactant capped CoFe2O4 nanoparticles. *Mater. Chem. Phys.* **130**, 1300–1306 (2011).
22. Ayyappan, S., Paneerselvam, G., Antony, M. P. & Philip, J. Structural stability of $ZnFe_2O_4$ nanoparticles under different annealing conditions. *Mater. Chem. Phys.* **128**, 400–404 (2011).
23. Yoo, H.-I. Phase stability and ionic transference number of a ferrite spinel, $Mn_{0.54}Zn_{0.35}Fe_{2.11}O_4$. *Solid state ion*. **84**, 77-88 (1996).
24. Mazarío, E., Herrasti, P., Morales, M. P. & Menéndez, N. Synthesis and characterization of $CoFe_2O_4$ ferrite nanoparticles obtained by an electrochemical method. *Nanotechnology* **23**, 355708 (2012).
25. Kim, Y. I., Kim, D. & Lee, C. S. Synthesis and characterization of CoFe2O4 magnetic nanoparticles prepared by temperature-controlled coprecipitation method. *Phys. B Condens. Matter* **337**, 42–51 (2003).
26. Cernea, M., Galizia, P., Ciuchi, I. -V., Aldica, G., Mihalache, V., Diamandescu & L. Galassi, C. $CoFe_2O_4$ magnetic ceramic derived from gel and densified by spark plasma sintering. *J. Alloys Compd.* **656**, 854–862 (2016).
27. Imine, S., Shoenstein, F., Mercone, S., Zaghrioui, M., Bettahar, N. & Jouini, N. Bottom-up and new compaction processes: A way to tunable properties of nanostructured cobalt ferrite ceramics. *J. Eur. Ceram. Soc.* **31**, 2943–2955 (2011).
28. Aubert, A., Loyau, V., Mazaleyrat, F. & LoBue, M. Uniaxial anisotropy and enhanced magnetostriction of $CoFe_2O_4$ induced by reaction under uniaxial pressure with SPS. *J. Eur. Ceram. Soc.* **37**, 3101–3105 (2017).
29. Millot, N., Le Gallet, S., Aymes, D., Bernard, F. & Grin, Y. Spark plasma sintering of cobalt ferrite nanopowders prepared by coprecipitation and hydrothermal synthesis. *J. Eur. Ceram. Soc.* **27**, 921–926 (2007).
30. Wu, L. N., Jiang, L. Z. & Hong, F. Y. Dielectric and Magnetic Properties of Sintered Cobalt Ferrite Derived from Nanocrystalline Powders. *Adv. Mater. Res.* **476–478**, 726–729 (2012).
31. Munir, Z. A., Anselmi-Tamburini, U. & Ohyanagi, M. The effect of electric field and pressure on the synthesis and consolidation of materials: A review of the spark plasma sintering method. *J. Mater. Sci.* **41**, 763–777 (2006).
32. Suarez, M., Fèrnandez, A., Menèndez, J. L., Torrecillas, R., Kessel, H. U., Hennicke, J., Kirchner, R., Kessel, T.

Challenges and Opportunities for Spark Plasma Sintering: A Key Technology for a New Generation of Materials. Sintering Applications, *InTech*, (2013). doi:10.5772/53706.
33. Maglia, F., Tredici, I. G. & Anselmi-Tamburini, U. Densification and properties of bulk nanocrystalline functional ceramics with grain size below 50 nm. *J. Eur. Ceram. Soc.* **33**, 1045–1066 (2013).
34. Anselmi-Tamburini, U., Garay, J. E. & Munir, Z. A. Fast low-temperature consolidation of bulk nanometric ceramic materials. *Scr. Mater.* **54**, 823–828 (2006).
35. Song, Q. & Zhang, Z. J. Shape Control and Associated Magnetic Properties of Spinel Cobalt Ferrite Nanocrystals. *J. Am. Chem. Soc.* **126**, 6164–6168 (2004).
36. Lu, L. T.,Dung, N. T., Tung ì, L. D., Thanh C. T., Qui, O. K., Chuck, N. V., Maenosono, S. & Thanh, N. T. K. Synthesis of magnetic cobalt ferrite nanoparticles with controlled morphology, monodispersity and composition: the influence of solvent, surfactant, reductant and synthetic conditions. *Nanoscale* **7**, 19596–19610 (2015).
37. Pechini, M. P. Method of preparing lead and alkaline earth titanates and niobates and coating method using the same to form a capacitor. (1967).
38. Khanam, S., Zakaria, A. K. M., Ahsan, M. H., Datta, T.K., Aktar, S., Liba, S. I., Hossain, S., Das, A. K., Kamal I., Yunus, S. M., Saha, D. K. & Erikkson, S.-G. Study of the Crystallographic and Magnetic Structure in the Nickel Substituted Cobalt Ferrites by Neutron Diffraction. *Mater. Sci. Appl.* **6**, 332–342 (2015).
39. Pugh, B. K., Kramer, D. P. & Chen, C. H. Demagnetizing Factors for Various Geometries Precisely Determined Using 3-D Electromagnetic Field Simulation. *IEEE Trans. Magn.* **47**, 4100–4103 (2011).
40. Pawley, G. S. Unit-cell refinement from powder diffraction scans. *J. Appl. Crystallogr.* **14,** 357–361 (1981).
41. Maaz, K., Mumtaz, A., Hasanain, S. K. & Ceylan, A. Synthesis and magnetic properties of cobalt ferrite (CoFe2O4) nanoparticles prepared by wet chemical route. *J. Magn. Magn. Mater.* **308**, 289–295 (2007).
42. Toksha, B. G., Shirsath, S. E., Patange, S. M. & Jadhav, K. M. Structural investigations and magnetic properties of cobalt ferrite nanoparticles prepared by sol–gel auto combustion method. *Solid State Commun.* **147**, 479–483 (2008).
43. Fariñas, J. C., Moreno, R., Pèrez, A., Garcìa, M. A., Garcìa-Hernàndez, M., Salvador, M. D. & Borrell, A. Microwave-assisted solution synthesis, microwave sintering and magnetic properties of cobalt ferrite. *J. Eur. Ceram. Soc.* **38**, 2360–2368 (2018).